Proceedings of FUELCELL2006
The 4th International Conference on FUEL CELL SCIENCE, ENGINEERING and TECHNOLOGY
June 19-21, 2006, Irvine, CA

FUELCELL2006-97164

PERFORMANCE EVALUATION OF A THERMALLY INTEGRATED FUEL CELL SYSTEM IN THE PRESENCE OF UNCERTAINTIES

Vasilis Tsourapas, Jing Sun
Department of Naval Architecture and Marine Engineering
University of Michigan
Ann Arbor, Michigan 48109
Email: djvas@umich.edu, jingsun@umich.edu

Anna Stefanopoulou
Department of Mechanical Engineering
University of Michigan
Ann Arbor, Michigan 48109
Email: annastef@umich.edu

ABSTRACT

In this work, we focus on robustness analysis of an integrated fuel cell and fuel reforming (FCFR) system, which relies on a feedback controller to mitigate hydrogen starvation and temperature overshoot during load transitions. The fuel reformer is used to process natural gas into a hydrogen rich flow to be utilized in a proton exchange membrane fuel cell (PEM-FC). The feedback controller uses the catalytic burner (CB) and the catalytic partial oxidizer (CPOX) temperatures as measurements and adjusts the air and fuel actuator commands to assure fast load following and high steady state efficiency. Several uncertainty sources which can potentially lead to closed loop performance deterioration are considered, including CPOX clogging, hydro-desulphurizer (HDS) clogging, fuel uncertainty and CB parameter uncertainty. Steady state and transient performance are analyzed for the different uncertainty scenarios, for both open and closed loop operation (i.e., with and without feedback control). The robustness of load following and CPOX temperature regulation of the closed loop system (feedforward and feedback controlled) is established, while the open loop system (feedforward controlled) is shown to be vulnerable to all sources of uncertainties considered.

INTRODUCTION

Integrated fuel cell and fuel reforming (FCFR) systems provide highly efficient and versatile solutions for mobile and stationary power applications. An FCFR system, investigated in our previous work [1], was formed by adding a catalytic burner (CB) in the outlet of a proton exchange membrane (PEM) fuel cell (FC). The CB utilizes the excess hydrogen in the FC to preheat the inlets of the catalytic partial oxidizer (CPOX) reformer. A dynamic model of the resulting thermally integrated FCFR system was developed and used to analyze the transient behavior and to identify the key parameters that affect its load following capabilities. A schematic of the system is given in Figure 1, where the corresponding dynamic states included in the model are also shown. Feedback control design and closed loop analysis, also performed in [1], resulted in improving the system performance and in mitigating hydrogen starvation and reactor overheat issues during transients. The feedback controller uses the measurements of the CPOX and CB temperatures and yields the time optimal actuator control signals. In order to implement the state feedback design, an observer (i.e., a model of the system) is incorporated to provide the state information for the feedback controller. Since the model of the system is embedded in the controller, any modeling error could affect the closed loop operation and may lead to performance deterioration and even system instability. In addition, other uncertainties, such as component aging, are inevitable and will lead to change in the system characteristics. Thus, it is important to evaluate the robustness of the feedback scheme for different uncertainty scenarios.

In this paper, several uncertainty sources are considered and their effects are analyzed. First, the robustness of the control scheme is validated against clogging of the CPOX and the hydro-desulfurizer (HDS) reactors. Clogging is a common phenomenon due to carbon deposition caused by aging or occasional overheating. Clogging increases the resistance of the re-

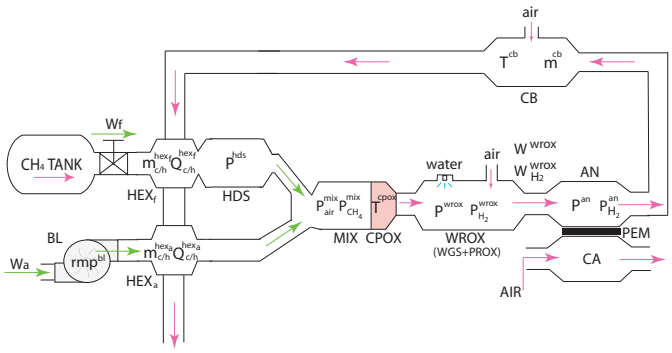

Figure 1. FCFR SYSTEM SCHEMATIC AND MODEL STATES

actor volume, thereby leading to increased pressure drop. Other consequences of clogging, such as catalyst deactivation, are not considered in this work. Uncertainty in the fuel composition is another concern, especially for mobile applications where fuel sources are unpredictable. The open and closed loop system performance will be evaluated and compared for three different compositions of the natural gas. Finally, since the controller utilizes the CB temperature as a measurement to predict the system response and provide the actuator commands, parameter uncertainty or measurement error can cause mismatch between actual and predicted response, leading to performance deterioration. Thus, the effect of uncertainty in the parameters of the CB is also examined.

Our analysis in this paper will show that the feedback design pursued in our earlier work is indeed robust against these uncertainties. Mechanisms that lead to the robust performance will also be explored to provide insight to the controller operation.

FCFR MODEL OVERVIEW

The FCFR system investigated in this work, shown in Figure 1, is composed of five main reactors, namely, the hydrodesulfurizer (HDS), the catalytic partial oxidizer (CPOX), the water gas shift (WGS), the preferential oxidizer (PROX) and the catalytic burner (CB). A 200kW proton exchange membrane FC (PEM-FC) is the power source of the plant. Natural gas, rich in methane CH_4, is supplied to the fuel reformer (FR) from a tank and is reformed into a rich H_2 flow. All FCFR components operate at low pressures of up to 110 kPa.

A 19-state nonlinear, control-oriented, dynamic model of the FCFR system is developed in order to analyze its behavior [1,2]. The dynamic states of the model are indicated inside the volumes in Figure 1 while other important variables are also shown such as the mass flow rates W_f, W_a, W^{wrox} and $W^{wrox}_{H_2}$ (see nomenclature definitions in Appendix). In [3], the initial model of the fuel processor was developed. The model in [3] assumed constant inlet temperature and did not include the heat exchangers and the catalytic burner.

Some important assumptions about the developed model include that all gases obey the ideal gas law and that each reactor was modeled as a lumped parameter volume with homogenous pressure and temperature distribution. The model is not suitable for start up or shut down simulations since such dynamics were not included. Finally, the model and its operating setpoints are valid for the range of FC loads between 20 to 80% (i.e. 50-160kW or 70-250A). Within this range of loads the FC stack voltage varies between 0.71V and 0.64V per cell with a total of 1000 0.04m^2 cells [4].

A brief description of the system operation is given in the this section with the governing dynamic equations summarized in Table 2 in the Appendix. The calculations for the chemical reactions in the CPOX and more details on the modeling can be found in [1,2,4].

The fuel flow into the system is defined based on the valve command u_f and (A7). The main air flow is supplied to the system by a blower (BL) which draws humidified air. The blower speed in revolutions per minute (rmp) is calculated via (A6) as a function of the air command u_a. Using the calculated blower speed and the blower map, the air flow is determined. The air and the fuel are pre-heated in separate heat exchangers (HEX). The HDS is used to remove the sulfur from the fuel flow [5,6]. In this work, only pressure dynamics are considered in the HDS (A11). The dynamic states in the HEX include mass (A8) and heat (A9). Then, the two flows are mixed in the mixer (MIX) where the partial pressure dynamics of the CH_4 (A12) and the air (A13) are taken into account. The mixture is then passed through the catalytic partial oxidizer (CPOX) where CH_4 reacts with oxygen to produce H_2. There are two main exothermal chemical reactions taking place in the CPOX: partial oxidation (POX) and total oxidation (TOX) [7,8] given in the following equations with their corresponding energy released per mole of reactant (ΔH^0).

$$(POX) \quad CH_4 + \tfrac{1}{2}O_2 \rightarrow CO + 2H_2$$
$$\Delta H^0_{pox} = -0.036\times10^6 \text{ J/mol} \qquad (1)$$
$$(TOX) \quad CH_4 + 2O_2 \rightarrow CO_2 + 2H_2O$$
$$\Delta H^0_{tox} = -0.8026\times10^6 \text{ J/mol.} \qquad (2)$$

Hydrogen is produced only by the POX reaction while heat is mostly generated by the TOX reaction. As shown in Fig. 2, the distribution between the two is dictated by the reactor temperature T^{cpox} (A15) and the molar flow ratio of O_2 to CH_4 in the MIX:

$$\lambda_{O2C} = P^{mix}_{O_2} / P^{mix}_{CH_4}. \qquad (3)$$

Moreover, since the CPOX products are also highly dependent

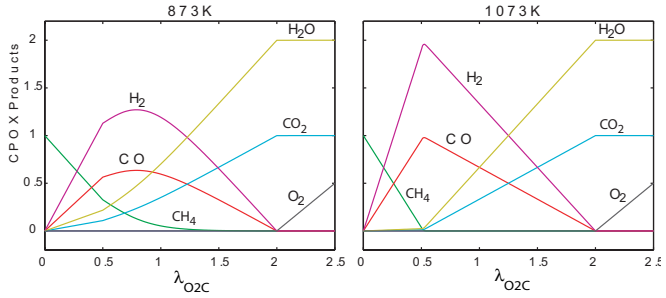

Figure 2. CPOX PRODUCTS AS A FUNCTION OF λ_{O2C} AND T^{cpox}

on the CPOX reactor temperature T^{cpox}, the optimum balance between the two reactions has to be determined.

Carbon monoxide (CO) is also created along with H_2 in the POX reaction, as can be seen in (1). Since CO poisons the PEM fuel cell catalyst, it has to be eliminated using water in the water gas shift reactor (WGS) and air in the preferential oxidizer (PROX). The latter are assumed to operate perfectly thus eliminating all the CO in the stream. In the model the PROX and WGS reactors are merged in one volume called the WROX where the total pressure dynamics (A16) and the H_2 partial pressure dynamics (A17) are included. The H_2-rich mixture leaving the WROX enters the anode of the fuel cell stack where the electrochemical reaction takes place to convert H_2 to electrical power.

The anode model includes the total pressure and the H_2 partial pressure dynamics, specified in (A18) and (A19) respectively. The reacting H_2 is given as a function of the demanded load (A20) and the resulting voltage as a function of H_2 pressure and the demanded load (A21). In this work, the demanded load refers to the total current drawn from the FC (I_{st}). The flow from the anode is then supplied to the catalytic burner (CB) where the excess H_2 is burnt using the air supplied through a blower. The temperature dynamics in the CB is given in (A24), where the heat released from burning the H_2 is a function of the air-to-H_2 stoichiometry in the CB (A26). Finally, the flow from the CB is fed to two separate heat exchangers (HEX - hot side), one to preheat the air and another to preheat the fuel flows before they enter the CPOX. This results in increased fuel utilization of the system.

The model (without the CB) has been verified with a higher order detailed model [4] while the CB model trends and qualitative response have also been verified [9].

FEEDFORWARD (FF) VS. COMBINED FEEDFORWARD AND FEEDBACK (FF-FB) OPERATION

To achieve maximum steady state efficiency, the following cost function, which represents the inverse of the system efficiency, is minimized with respect to the air and fuel commands

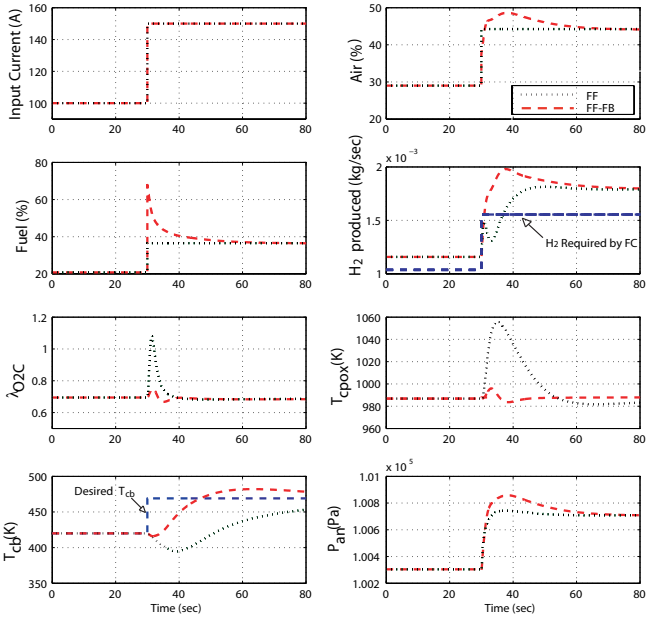

Figure 3. SYSTEM RESPONSE WITH FF AND FF-FB CONTROL

(u_a^*, u_f^*):

$$\min_{u_a,u_f} \left(\frac{Q_{LHV} W_{fuel}^{consumed}}{V_{st} I_{st}} \right). \tag{4}$$

for each FC load. This optimization yields the static maps for u_a^* and u_f^*, as functions of the demanded load, that can be used as a feedforward control to achieve desired steady state setpoints for the control commands. However, utilizing only this feedforward (FF) map, the load following capabilities and temperature regulation characteristics of the system were shown to be poor during transients, as shown in Figure 3. The hydrogen production in FF operation has a significant undershoot that causes hydrogen starvation in the anode of the FC while the temperature in the CPOX has a large overshoot which could damage the CPOX reactor. The main reason for this transient performance is the fuel chocking during a transient [1]. When the fuel enters the MIX, it is chocked by the air flow due to its substantially smaller flow rate compared to the air causing the λ_{O2C} to increase and in turn the hydrogen production to drop and CPOX temperature to overshoot (based on Figure 2). Furthermore, with FF control the system cannot tolerate uncertainties for steady state operation, for example the CPOX temperature will not be kept constant if there is an increase in the CPOX pressure drop as shown in the following section. A rate limiter of 5A/sec could prevent hydrogen starvation and CPOX temperature overshoot with the use of a FF controller only, which can be easily implemented. If faster load following capabilities and more robust performance are required,

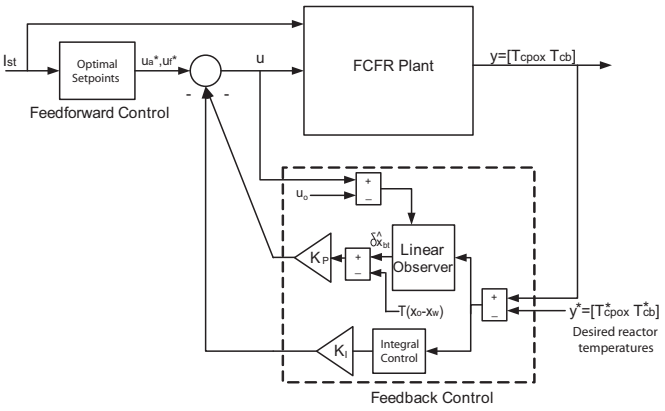

Figure 4. FF-FB CONTROL SCHEMATIC

a combined FF-FB control scheme has to be utilized.

To improve the load following capabilities and prevent hydrogen starvation and CPOX overheating, design of a feedback controller is pursued in [1]. The choice of feedback measurements y as T_{cpox} and T_{cb} was made by taking into account the ease of the measurements and the number of required sensors. In addition, the CPOX temperature was used since we are interested in regulating it, while the CB temperature was used since it provides a virtual hydrogen sensor. By measuring T_{cb} we can estimate, using the model, the total amount of hydrogen produced.

A schematic of the designed feedback controller is given in Figure 4. Details on the design of the controller and the derivation of the control law can be found in [1]. Both the hydrogen starvation and the temperature overshoot were mitigated with the application of the controller as shown in Figure 3. Note that the controller includes integrator states for the difference between the actual and the desired values of T_{cpox} and T_{cb} in order to achieve zero error steady state regulation.

One issue with the feedback controller, since it is observer-based and embeds the plant model in the controller, is whether it can tolerate changes in the plant and still perform satisfactory as far as starvation protection and temperature regulation are concerned. This issue will be addressed for several representative scenarios.

ROBUSTNESS AGAINST CPOX CLOGGING

A well-known problem for CPOX systems is clogging due to carbon build up and deformation caused by the aging process and occasional excess temperature. Risk of CPOX clogging due to carbon formation is increased when reforming diesel or gasoline fuels, because of their heavy carbon concentration, but is still an issue when reforming natural gas. Deformation of the CPOX catalyst can easily occur if the CPOX temperature exceeds the meltdown temperature of the catalyst or backbone material (1000-1100 K), which can be caused by large λ_{O2C} values [10].

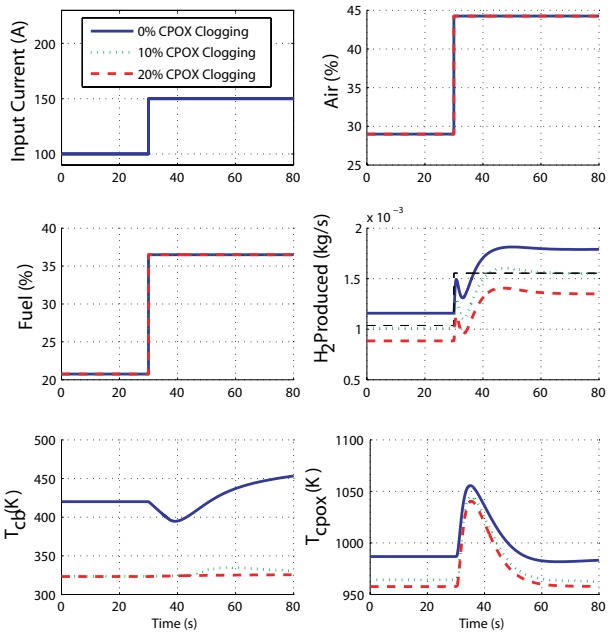

Figure 5. SYSTEM RESPONSE WITH FF CONTROL FOR VARIOUS CPOX CLOGGING

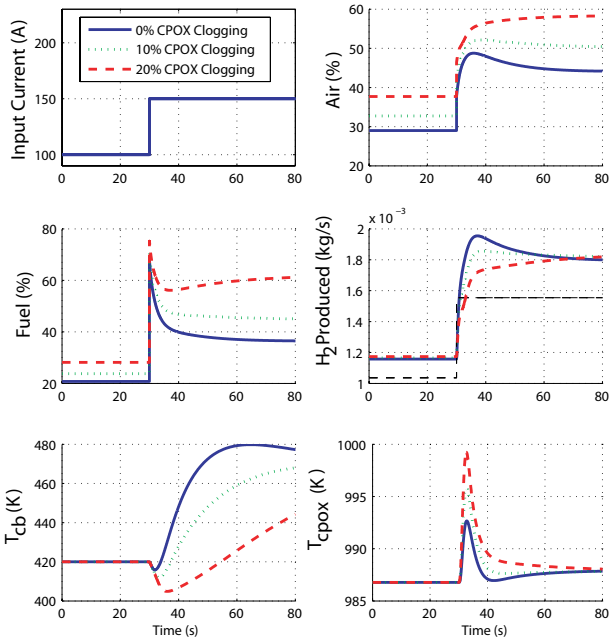

Figure 6. SYSTEM RESPONSE WITH FF-FB CONTROL FOR VARIOUS CPOX CLOGGING

Note that catalyst deactivation effects due to carbon formation are not considered in this work, which may compound to the adverse effects of CPOX clogging.

Clogging of the CPOX reactor leads to increased CPOX pressure drop that can be emulated in our numerical simulation

model by a reduction in the CPOX outlet effective orifice area. Given the low operating pressure of the system examined in this work, even small increase in the CPOX reactor pressure drop can affect the reactant flows and hence the hydrogen produced by the FR. Figure 5 shows the effect of CPOX clogging to the FF controlled FCFR system. Even at 10% CPOX clogging the amount of hydrogen produced by the reformer is less than the amount required by the fuel cell, leading to prolonged hydrogen starvation. Furthermore, there is a significant increase in the CPOX temperature overshoot caused by the increased λ_{O2C} overshoot. CPOX temperature overshoot increases from 68 K (0% CPOX clogging) to 87K (20% CPOX clogging). Even though both fuel and air flows are clogged equally with the CPOX clogging, the fuel chocking problem observed in the nominal plant (0% CPOX clogging) is amplified. This can be attributed to the increase in the CPOX and MIX pressure from 104.73 kPa to 105.81 kPa, which in turn causes increased resistance in the incoming fuel flow. Finally, the CB temperature is reduced dramatically due to the prolonged anode hydrogen starvation (i.e., no hydrogen entering the CB).

Figure 6 shows the response of the FCFR system when combined FF and FB control are applied. Mainly due to the integral action of the control scheme, the steady state values of CPOX temperature and hydrogen production are regulated to the desired value (the same value as for 0% CPOX clogging) for all levels of CPOX clogging. The transient response of CPOX temperature deteriorates significantly, when compared to the nominal FB response, but is kept under 1000 K. The starvation period (SP)[1] is also kept within satisfactory limits and degrades from 0.9sec (0% CPOX clogging), to 3.6sec (20% CPOX clogging).

The FF-FB control scheme mitigates the effects of CPOX clogging during steady state by shifting the air and fuel operating setpoints in order to achieve the desired CPOX temperature and hydrogen production. During transient operation, the controller increases the overshoot of fuel and slows down air in order to mitigate the increase in CPOX temperature overshoot.

ROBUSTNESS AGAINST HDS CLOGGING

In the open loop analysis of the system, the HDS volume in the fuel flow path upstream of the mixer was identified as the main cause of the poor load following performance of the system [1]. Due to the relatively large volume of the HDS and smaller fuel flow rate (kg/s) compared to that of air, the fuel was restricted from entering the MIX during load transitions, therefore causing hydrogen production delay. In this section the system performance is evaluated under different levels of HDS clogging.

Utilizing only the feedforward map, the open loop system response is shown in Figure 7 for 0%, 10% and 20% HDS clogging. It can be seen that the system cannot operate open loop with 10% or more HDS clogging, since the steady state hydrogen production is less than the demanded amount by the fuel cell. Furthermore, the high CPOX temperature caused by the HDS clogging would cause melt down of the CPOX reactor.

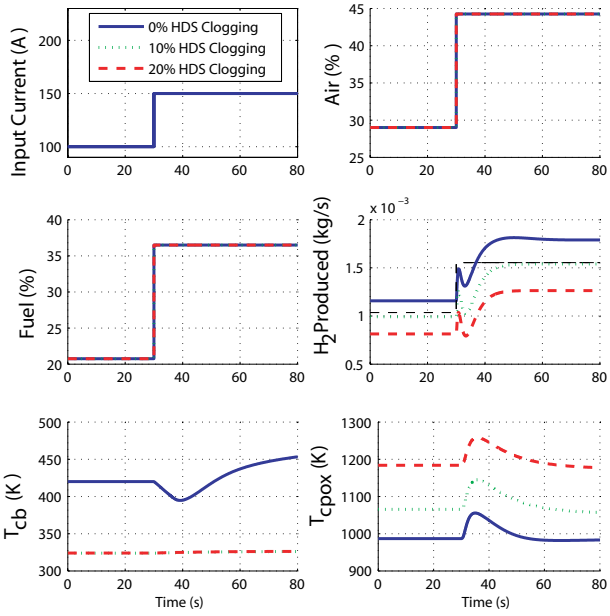

Figure 7. SYSTEM RESPONSE WITH FF CONTROL FOR VARIOUS HDS CLOGGING

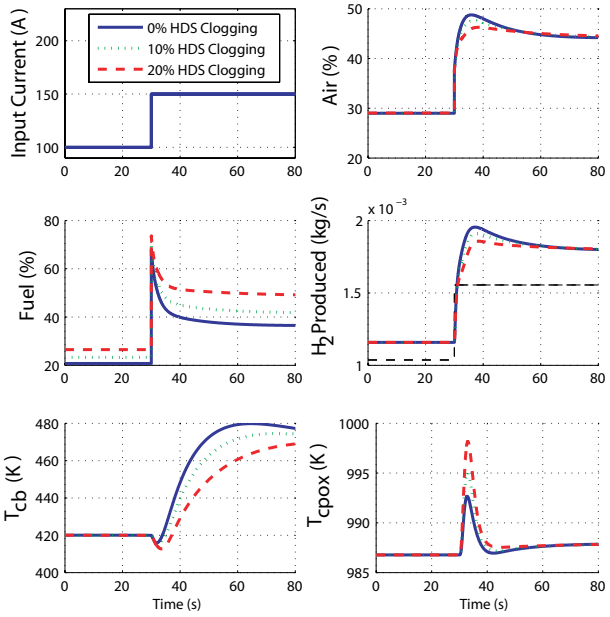

Figure 8. SYSTEM RESPONSE WITH FF-FB CONTROL FOR VARIOUS HDS CLOGGING

[1]SP is defined as the period during a load transition where the demanded amount of hydrogen is higher than the amount of hydrogen produced.

Contrary to the CPOX clogging case where both air and fuel flows are affected, only the fuel flow is restricted with the HDS clogging. The resulting response though is similar due to the increase in the MIX pressure from 104.73 kPa to 104.97 kPa. Note that in the CPOX clogging case the pressure increase is larger given that the flow out of the CPOX is the sum of the air and fuel flows entering. That explains why at 20% CPOX clogging, the FF-FB system performance exhibits increased deterioration compared to 20% HDS clogging. Again, there is a significant increase in the FF CPOX temperature overshoot, which is a result of the increased λ_{O2C} overshoot (i.e., increased fuel chocking). At 20% HDS clogging the CPOX temperature overshoot is 78 K while for the nominal plant it is 68 K.

When the FF-FB controller is applied, the system exhibits satisfactory performance both in steady state operation and during the transient. The steady state performance is achieved by increasing the fuel command as the HDS clogging gets worse, while the air command at steady state remains unchanged. The transient performance is restored by increasing the overshoot in the fuel and slowing down the air command, thus overcoming the increased fuel chocking. The CPOX temperature is maintained below 1000 K during the transient.

ROBUSTNESS AGAINST CB PARAMETER UNCERTAINTY

Since the CB temperature is a critical measurement in the designed feedback controller, it is important to ensure the robustness of the system against uncertainty of the CB model parameters. The dynamic response of the CB temperature is mainly a function of its mass and heat capacity constants, namely the parameter $\phi_{cb} = m_{bed}^{cb} c_{Pbed}^{cb}$. The nominal value of ϕ_{cb} used in the model and in the observer design is based on approximate data (m_{bed}^{cb}=10 kg, c_{Pbed}^{cb}=500 J/kgK, ϕ_{cb}=5000 J/K [9]). Estimation of the heat capacity or the mass of a reactor can vary significantly based on whether the catalyst, the pipes or the shell of the reactor are taken into account.

In this section we examine whether the system performance is affected when varying ϕ_{cb}. Figures 9 and 10 show the response of the plant with $0.8\phi_{cb}$, ϕ_{cb} and $1.2\phi_{cb}$ during a 100-150A load step change with FF and FF-FB. The hydrogen starvation period and the maximum CPOX temperatures remain practically unchanged in all three cases for both control schemes.

Even thought with FF control the response time of T_{cb} varies when ϕ_{cb} changes, the FF-FB performance is not affected. More investigation is required to fully quantify the FB robustness to this CB thermal-capacity uncertainty and will be included in future work. The results from this understanding can be also applied to uncertainty in temperature sensor dynamics especially during start-up.

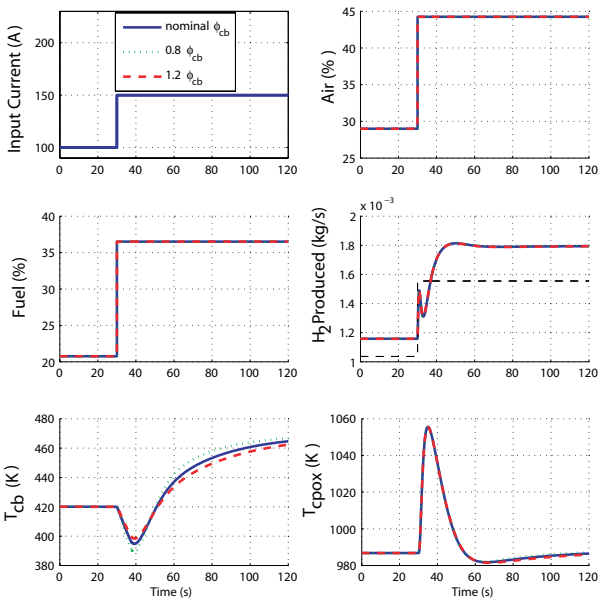

Figure 9. SYSTEM RESPONSE WITH FF CONTROL FOR VARIOUS ϕ_{cb}

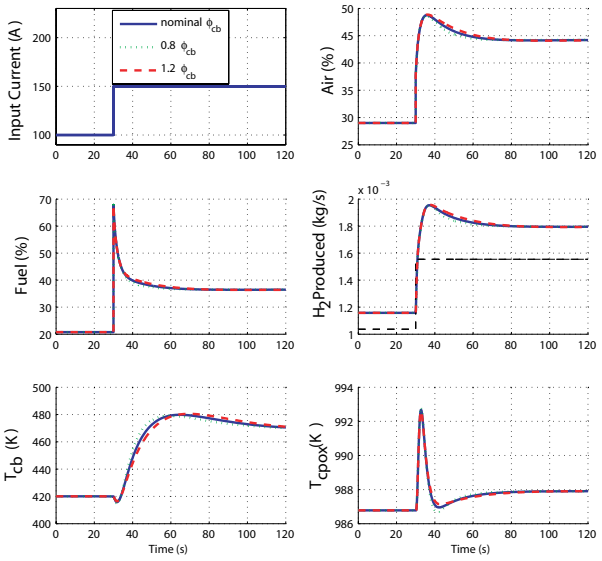

Figure 10. SYSTEM RESPONSE WITH FF-FB CONTROL FOR VARIOUS ϕ_{cb}

ROBUSTNESS AGAINST FUEL COMPOSITION UNCERTAINTY

The initial analysis of the system was done using a 100% pure methane natural gas fuel. Natural gas consists of 87% to 96% (molar ratio) of methane and normally includes small amounts of ethane, propane and nitrogen. Traces of butane, pentane, hexanes, carbon dioxide and hydrogen can also be found in natural gas [11]. The exact fuel composition varies depending

Table 1. FUEL COMPOSITIONS EXAMINED

(Mole %)	Fuel 1	Fuel 2	Fuel 3
CH_4	100	87.0	94.9
C_2H_6	0	5.2	2.5
C_3H_8	0	1.9	0.7
N_2	0	5.6	1.6
Other	0	0.3	0.3

on the place of fueling and after-treatment methods applied to the extracted natural gas. The effects of variable natural gas composition have been studied extensively in direct injection engines and have been found to have a big effect in ignition delay and peak temperature [12]. The performance of the fuel cell based system under investigation is also greatly affected in terms of the hydrogen production and CPOX temperature as shown here.

Using an equilibrium Gibbs minimization reactor, as in the initial model, it is verified that the CPOX reaction products as a function of the O_2/C ratio defined for the new fuel do not change for the same temperature conditions. Thus, the same maps can be employed (as in Figure 2). The fact that no fuel component other than methane is found in the output products, even at low λ_{O2C} ratios, can be explained by the relatively large methane content in the fuel (>87%) and increased selectivity of ethene and propane against methane in the oxidation reaction (i.e., ethane and propane are oxidized first) [13]. The fact that the maps are the same, though, does not guarantee the same hydrogen production due to the potential different equilibrium temperature when using the predetermined feedforward maps for air and fuel commands (i.e. same air and fuel flows for variable fuel compositions).

In order to account for variable composition in the reformer mixture, the CPOX temperature dynamics are now expressed as

$$\frac{dT^{cpox}}{dt} = \frac{1}{m^{cpox}c_P^{cpox}}[W^{cpox}(c_P^{mix}(T^{mix}-T_{ref}) - \\ -c_P^{cpox}(T^{cpox}-T_{ref}))+\Delta H^0] \qquad (5)$$

where the heat capacity of the incoming flow from the mixer, c_P^{mix}, is now a weighted sum of all the species in the fuel and air composition while the enthalpy of formation of the inlets minus the products, ΔH^0, also takes into account the ethane, propane and other species in the fuel. The fuels examined in this work are given in Table 1, where "*Other*" indicates traces of butane, pentane and oxygen. The corresponding steady state and transient FF response of the system using these three fuels is given in Figure 11 while the closed loop in Figure 12.

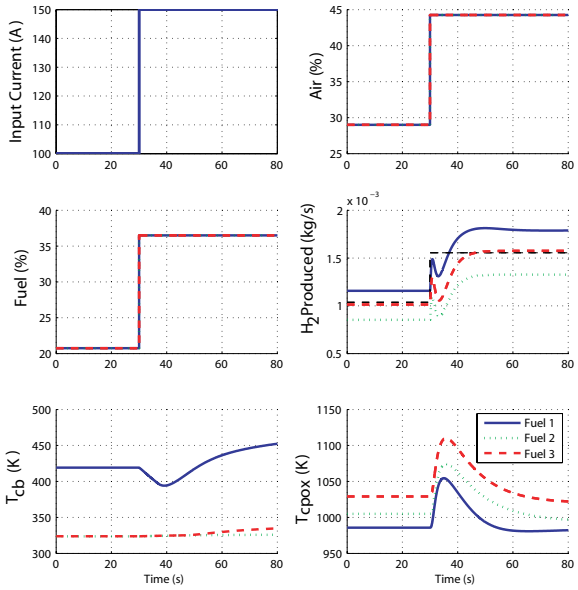

Figure 11. SYSTEM RESPONSE WITH FF CONTROL FOR VARIOUS FUELS

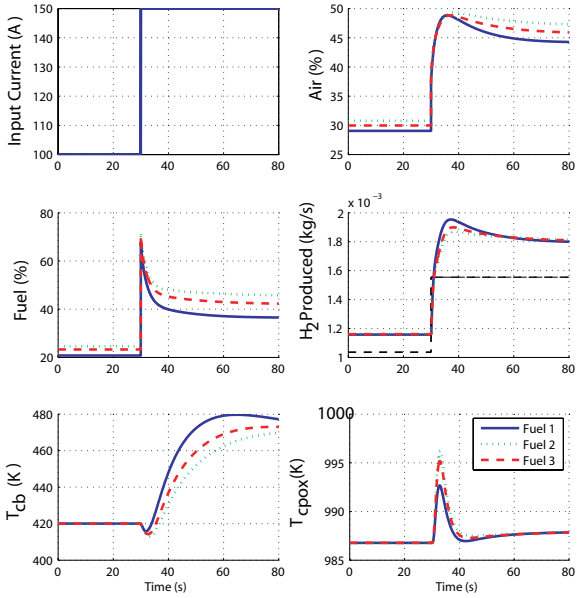

Figure 12. SYSTEM RESPONSE WITH FF-FB CONTROL FOR VARIOUS FUELS

In Figure 11, the FF controlled scheme exhibits prolonged hydrogen starvation when *Fuel 2* and *Fuel 3* are used, while the CPOX temperature is also significantly increased for these fuels. Note, that the CPOX temperature overshoot remains constant, contrary to the previous scenarios examined and it is the steady state values that are mainly affected. This was also verified by examining the eigenvalue (pole) of equation 5 which remains con-

stant, for all three fuels, i.e., the thermal capacity of the mixture is practically constant since methane content is large in all fuels.

The FF-FB performance with all three fuels is acceptable as far as hydrogen and CPOX temperature responses are concerned. The degradation of the SP is negligible while the deterioration in CPOX temperature overshoot is small and can be attributed to the slight increase in reformer pressure due to the shifted air and fuel commands. Thus, the ability of the controller to provide an acceptable performance can be attributed mainly to the integral action.

CONCLUSIONS

In this work, the effects of four representative uncertainty sources are considered and performance of the FCFR system is evaluated under FF and FF-FB control. It is found that the designed feedback control scheme, which measures T_{cb} and T_{cpox}, is able to regulate the hydrogen production and safeguard the CPOX reactor from large temperature overshoots under these scenarios. The integrator terms manage to maintain the steady state values to the desired levels while the controller coordinates the air and fuel actuators during load transitions in order to achieve satisfactory load following capabilities and temperature regulation. For future work, the tolerance of the system with catalyst deactivation effects included will be examined in the case of CPOX clogging and the mechanisms with which the feedback system assures robustness in the presence of CB uncertainties will be further explored.

REFERENCES

[1] V. Tsourapas, J. Sun, and A. Stefanopoulou. Dynamics, optimization and control of a fuel cell based combined heat power (chp) system for shipboard applications. *American Control Conference*, 2005.

[2] V. Tsourapas, J. Sun, and A. Stefanopoulou. Modeling and dynamics of a fuel cell combined heat power system for marine applications. *IASME Transactions*, 2(1):287–293, 2004.

[3] J.T. Pukrushpan, A.G. Stefanopoulou, and S. Varigonda. Control-oriented model of fuel processor for hydrogen generation in fuel cell applications. *IFAC Symposium on Advances in Automotive Control*, April 2004.

[4] Jay Tawee Pukrushpan, Anna Stefanopoulou, and Huei Peng. *Control of Fuel Cell Power Systems : Principles, Modeling, Analysis and Feedback Design*. Springer, 1st edition, 2004.

[5] A.L. Dicks. Hydrogen generation from natural gas for the fuel cell systems of tomorrow. *Journal of Power Sources*, 61:113–124, 1996.

[6] T.H. Gardner, D.A. Berry, K.D. Lyons, S.K. Beer, and A.D. Freed. Fuel processor integrated H_2S catalytic partial oxidation technology for sulfur removal in fuel cell power plants. *Fuel*, 81:2157–2166, 2002.

[7] A.L. Larentis, N.S. de Resende, V.M.M. Salim, and J.C. Pinto. Modeling and optimization of the combined carbon dioxide reforming and partial oxidation of natural gas. *Applied Catalysis*, 215:211–224, 2001.

[8] J. Zhu, D. Zhang, and K.D. King. Reforming of CH_4 by partial oxidation: thermodynamic and kinetic analyses. *Fuel*, 80:899–905, 2001.

[9] *Communication with UTRC*, 2004.

[10] *Communication with SOFCo-EFS*, 2005.

[11] Union Gas website. Natural gas properties. *http://www.uniongas.com*.

[12] J. D. Naber, D. L. Siebers, S. S. Di Julio, and C. K. Westbrook. Effects of natural gas composition on ignition delay under diesel conditions. *Combustion and Flame, 99*, pages 192–200, 1994.

[13] Parag Adhangale and David Keffer. A grand canonical monte carlo study of the adsorption of methane, ethane, and their mixtures in one-dimensional nanoporous materials. *Langmuir, 18*, pages 10455–10461, 2002.

APPENDIX: FCFR model equations and nomenclature

Table 2. LIST OF GOVERNING EQUATIONS FOR FCFR MODEL

Description	*Equation*	
Newton's Law : BL	$\frac{drpm^{bl}}{dt} = \frac{1}{\tau_b}(\frac{u_a}{100} rpm^{bl}_{ref} - rpm^{bl})$	(A6)
Fuel flow inlet :	$W_f = \frac{u_f}{100} W_{nom} \sqrt{\frac{P_{tank} - P^f_{hex_c}}{\Delta P_{nom}}}$	(A7)
Conservation of Mass : HEX h/c sides	$\frac{dm^{hex_{h/c}}}{dt} = \Sigma W^{hex_{h/c}}_{in} - \Sigma W^{hex_{h/c}}_{out}$	(A8)
Conservation of Energy : HEX h/c sides	$\frac{dQ^{hex}_{h/c}}{dt} = \Sigma(W^{hex_{h/c}}_{in} c_{P_{in}}(T_{in} - T_{ref})) -$ $- \Sigma(W^{hex_{h/c}}_{out} c_{P_{out}}(T^{hex_{h/c}}_{out} - T_{ref})) \pm UA \cdot (LMTD)$	(A9)
Logarithmic Mean Temperature Difference	$LMTD = \frac{(T^{in}_h - T^{in}_c) - (T^{out}_h - T^{out}_c)}{ln\frac{(T^{in}_h - T^{in}_c)}{(T^{out}_h - T^{out}_c)}}$	(A10)
Ideal Gas Law : HDS	$\frac{dP^{hds}}{dt} = \frac{RT^{hds}}{M_{CH_4} V^{hds}}(W^{hex_f} - W^{hds})$	(A11)
Ideal Gas Law : MIX, CH_4	$\frac{dP^{mix}_{CH_4}}{dt} = \frac{RT^{mix}}{M_{CH_4} V^{mix}}(W^{hds} - x^{mix}_{CH_4} W^{cpox})$	(A12)
Ideal Gas Law : MIX, Air	$\frac{dP^{mix}_{air}}{dt} = \frac{RT^{mix}}{M_{air} V^{mix}}(W^{hex_a}_c - x^{mix}_{air} W^{cpox})$	(A13)
Static Temperature Relationship : MIX	$T^{mix} = \frac{c_{P_{CH_4}} W^{hds} T^{hds} + c_{P_{air}} W^{hex_a}_c T^{hex_a}_c}{c_{P_{CH_4}} W^{hds} + c_{P_{air}} W^{hex_a}_c}$	(A14)
Conservation of Energy : CPOX	$\frac{dT^{cpox}}{dt} = \frac{1}{m^{cpox} c^{cpox}_P}(W^{cpox}\left(c^{mix}_P(T^{mix} - T_{ref}) - c^{cpox}_P(T^{cpox} - T_{ref})\right) +$ $+ N_{CH_4 r}\left(S \cdot (-\Delta H^0_{pox}) + (1-S) \cdot (-\Delta H^0_{tox})\right) +$ $+ N_{O_2 r H_2 CO}\left(\beta \cdot (-\Delta H^0_{hox}) + (1-\beta) \cdot (-\Delta H^0_{cox})\right))$	(A15)
Ideal Gas Law : WROX	$\frac{dP^{wrox}}{dt} = \frac{RT^{wrox}}{M^{wrox} V^{wrox}}\left(W^{cpox} - W^{wrox} + W^{wgs}_{H_2O} + W^{prox}_{air}\right)$	(A16)
Ideal Gas Law : WROX, H_2	$\frac{dP^{wrox}_{H_2}}{dt} = \frac{RT^{wrox}}{M_{H_2} V^{wrox}}\left((1+\eta^{wrox}) W^{cpox}_{H_2} - x^{wrox}_{H_2} W^{wrox}\right)$	(A17)
Ideal Gas Law : AN	$\frac{dP^{an}}{dt} = \frac{RT^{an}}{M^{an} V^{an}}\left(W^{wrox} - W^{an} - W^{react}_{H_2}\right)$	(A18)
Ideal Gas Law : AN, H_2	$\frac{dP^{an}_{H_2}}{dt} = \frac{RT^{an}}{M_{H_2} V^{an}}\left(x^{wrox}_{H_2} W^{wrox} - x^{an}_{H_2} W^{an} - W^{react}_{H_2}\right)$	(A19)
H_2 reacts in FC	$W^{react}_{H_2} = M_{H_2} \frac{nI_{st}}{2F}$	(A20)
Voltage Calculation :	$V = N_{cell}\left(a_1 - a_2 \frac{I_{st}}{A_{cell}} - a_3\left(\frac{I_{st}}{A_{cell} P_{H_2}}\right)^2\right)$	(A21)

$$Ideal\ Gas\ Law:\ CB \qquad P^{hex_{h/c}} = \frac{1}{V^{hex_{h/c}}} \frac{m^{hex_{h/c}}}{M^{hex_{h/c}}} R T^{hex_{h/c}} \tag{A22}$$

$$Conservation\ of\ Mass:\ CB \quad \frac{dm^{cb}}{dt} = W^{an} + W^{aircb} - W^{cb} \tag{A23}$$

$$Conservation\ of\ Energy:\ CB \quad \frac{dT^{cb}}{dt} = \frac{1}{m^{cb}_{bed} c^{cb}_{Pbed}} (W^{an} c^{an}_P (T^{an} - T_{ref}) + + W^{aircb} c^{air}_P (T^{aircb} - T_{ref}) - W^{cb} c^{cb}_P (T^{cb} - T_{ref}) + Q^{cb}_r) \tag{A24}$$

$$Ideal\ Gas\ Law:\ CB \qquad P^{cb} = \frac{1}{V^{cb}} \frac{m^{cb}}{M^{cb}} R T^{cb} \tag{A25}$$

$$Heat\ released\ from\ H_2\ in\ CB\ Q^{cb}_r = \frac{Q^{H_2}_{LHV}}{M_{H_2}} \cdot min \left\{ W^{an}_{H_2}, \frac{W^{aircb}}{34.2} \right\} \tag{A26}$$

Table 3. NOMENCLATURE DEFINITIONS

Symbol	Description	Scripts/Acronyms	Description
A_{cell}	Area of each cell in FC stack	CH_4 or f	Methane
F	Farraday's Constant	H_2	Hydrogen
I_{st}	FC Current	O_2	Oxygen
M	Molar weight	*	Denotes Optimal/Desired Values
N_{cell}	Number of cells in FC stack	a	Air
P	Pressure	bed	Property of the reactor bed
Q	Heat	in	Incoming flow Property
Q_{LHV}	Lower Heating Value	nom	Nominal Value
Q_{obs}	Observability gramian	out	Outgoing flow Property
R	Gas Constant	ref	Reference Value
T	Temperature	FC	Fuel Cell
U_{H_2}	H_2 FC Utilization	FPS	Fuel Processor System
V	Volume	an/AN	Anode
W	Mass Flow	bl/BL	Blower
ΔH^0	Enthalpy of formation	cb/CB	Catalytic Burner
η	Efficiency	$cpox/CPOX$	Catalytic Partial Oxidizer
c_P	Specific Heat	hds/HDS	Hydro-Desulphurizer
m	Mass	$hex\ h/c\ /HEX$	Heat exchanger hot/cold side
u_a	Air Setpoint	mix/MIX	Mixer
u_f	Fuel Setpoint	$tank$	Tank
x	Mass fraction	$wrox/WROX$	Water Gas Shift & Preferential Oxidizer